Available online at www.sciencedirect.com
ScienceDirect
Journal of Sound and Vibration 319 (2009) 406–425
JOURNAL OF SOUND AND VIBRATION
www.elsevier.com/locate/jsvi

Excitation and sensing of multiple vibrating traveling waves in one-dimensional structures

Ran Gabai, Izhak Bucher*

Faculty of Mechanical Engineering, Technion-Israel Institute of Technology, Haifa, Israel

Received 7 August 2007; received in revised form 26 May 2008; accepted 7 June 2008
Handling Editor: A.V. Metrikine
Available online 29 July 2008

Abstract

Lightly damped vibrating structures normally exhibit vibration patterns that are a combination of standing waves, i.e. mode shapes. Traveling waves, on the other hand, occur only under special circumstances. In this work, the theoretical conditions under which traveling waves prevail in finite structure are investigated. These conditions are highly sensitive to the geometrical and material parameters of the structure and in particular the vibration pattern is sensitive to the boundary conditions. There are several combinations under which traveling waves cannot be formed and these ill-posed cases are analyzed in some detail. To overcome the unavoidable uncertainties in a model, a tuning process based on identification and optimization of the excitation is suggested. The identification process uses a parametric algorithm to estimate the wavenumbers of the measured vibrations. Then, the waves are decomposed into traveling and standing parts and the external excitation is tuned until a pure traveling wave is formed.

1. Introduction

Pure traveling vibration waves are usually observed on long or cyclically symmetric structures and seldom on normal finite structures [1]. Discontinuous segments, where the structural impedance changes abruptly, results in multiple reflection of waves that create a complex mixture of standing and traveling deformations. In some applications it is desired to deliberately create traveling deformation waves. Most of these applications use traveling waves to create propulsion, e.g. ultrasonic motors [2]; squeeze-film levitation and transportation devices [3], where a traveling pressure wave carries a levitated object along the direction of progression. In Robotics, snake-like structure that exhibits traveling waves create propulsion, steering and maneuvering in a viscous fluid environment [4]. In all these applications, it is desired to eliminate the standing waves while maintaining the traveling ones.

In a finite medium, the excited vibration waves are partially reflected upon hitting the boundaries. Thus, standing waves arise and they dominate the structural vibrations. Wave reflections occur when the incoming wave experiences an impedance change along its path [5]. A feedback control based approach, controlling the

*Corresponding author. Tel.: +972 4 8293153; fax: +972 4 8295711.
E-mail address: bucher@technion.ac.il (I. Bucher).

0022-460X/$ - see front matter © 2008 Elsevier Ltd. All rights reserved.
doi:10.1016/j.jsv.2008.06.013

vibrating waves along a beam, was investigated by Pines and von Flotow [6], by Mei [7] and also by Gardonio and Elliott [8]. Elliott and Billet [9] proposed a digital adaptive control method for flexural wave propagating along a beam. Traveling waves occur also on axially moving string systems (Tan and Ying [10]). Feedback control can eliminate these waves as presented by Chung and Tan [11]. Alternatively, several configurations and excitation methods were reported to excite traveling waves in finite structures. A passive method, matching the mechanical impedance of a vibrations absorber to the medium's characteristic impedance is described by Hull [12]. In this work, longitudinal traveling waves are crated in a bar and also proposed in Ref. [2] by Kuribayashi et al. for ultrasonic linear motors. A different approach was proposed in Ref. [13] by Loh and Ro, where two neighboring natural mode shapes are excited simultaneously by two forces at the same frequency but phased in time to create a response imitating a slowly modulated traveling wave. Tanaka and Kikushima [14] propose the active sink method where a pair of forces is applied at the boundaries while one acts as a source and the other as a sink. In this approach, the structure appears to the progressing waves as if it was infinite. The work presented by Minikes et al. [15] further develops this idea and adaptively tunes the external forces to overcome discrepancies between the theoretical and actual models. The tuning procedure is based on minimizing a scalar function describing the proportion of the traveling to standing waves in the measured vibration. Minikes et al. also pointed out the fact that for certain wavelengths, the tuning process fails to achieve pure traveling waves due to dynamical behavior of a redundant part of the structure. This paper adds some understanding and theoretical results that help in the active tuning procedure. The present work improves the wave identification method and thus improves the tuning process in the presence of multiple traveling waves. Gabai and Bucher [16], presented the basic theory of generating traveling waves, by applying forces at the boundaries. In Ref. [16], the main concepts are described both for one- and two-dimensional structures and the basic methodology of the tuning algorithm is outlined. The present paper advances the theory and the mathematical foundations of the making of traveling waves in vibrating structures. In particular, the dynamics of non-simple boundary conditions and their effect on the ability to generate perfect traveling waves are studied in detail both theoretically and experimentally.

The tuning process, that produces pure traveling waves, necessitates the identification of the vibrating wave characteristics from measurements of the instantaneous structural vibrations. A parametric wave identification and decomposition approach, based on fitting an ellipse to the measured vibrating response is described in Ref. [17]. This method can deal with waves that are dominated by a single wavelength. In Ref. [15], the ellipse tuning method is further developed showing how the wavelength can be extracted from the measurements and an additional method based on the non-parametric Hilbert transform is proposed. Other types of parametric methods that are based on the Prony method have been reported in Ref. [18], but these methods are highly sensitive to noise and to the number of selected parameters.

In this work, a method that has been previously employed for the Estimation of Signal Parameters via Rotational Invariance Techniques (ESPRIT) is adopted. This method was developed in Refs. [19,20]. The ESPRIT method is superior to other parametric methods that identify sinusoids embedded in noise, and it has better statistical accuracy over the similar-in-concept Prony-like methods [20]. ESPRIT is mainly used for frequency estimation of noisy sinusoids [21] and for Direction Of Arrival (DOA) estimation in radars [22]. In this work, the ESPRIT is used to estimate the dominant spatial wavelengths of the vibrating structure.

The ESPRIT identification method adds the possibility to tune several traveling waves having several wavelengths, simultaneously. In addition, the paper investigates the effect of imperfect modeling on the required excitation to produce traveling waves and its influence on the tuning procedure. In this work, a rather simple vibrating structure is considered—a taut vibrating string. A vibrating string keeps the mathematical expressions concise while the spirit of the analysis applies to general, one-dimensional structures, like beams. The focus is set on the traveling ingredient of the vibration and disregards non-progressive components (i.e. evanescent waves) which do not affect the traveling phenomenon away from the edges. The tuning procedure is completely independent of the physical model and it can handle complex vibrating structures exactly in the same manner.

The structure of this paper is as follows: after the introduction, wave identification methods are described in Section 2. In this part, several methods for wave characterization including the ESPRIT, are detailed. Later, the theoretical background of the active boundary conditions under which traveling waves are formed is outlined and various boundary models are analyzed. The effect of uncertainty in the parametric model of the

structure on the forming of traveling wave is then studied. Section 4 discusses the traveling wave tuning algorithm and finally, a series of experiments is shown and analyzed.

2. Waves identification—estimating waves parameters from measurements

The identification and separation of the vibrations in terms of waves is a key element when trying to generate a traveling deformation. It is necessary to evaluate the existing composition of the structure's vibrations from measurements and decompose the traveling and standing waves portions of the response. The process of wave identification involves the execution of tempo-spatial measurements from which the waves' coefficients and wavelengths are extracted. In this section, wave decomposition and two parametric methods for wave identification are briefly introduced.

2.1. Traveling and standing waves decomposition

Initially, a wave with a single wavelength is discussed. This type of response represents general steady state vibrations of a 1D structure under a single excitation frequency, ω:

$$u(x,t) = U(x)q(t) = [C_1 e^{-i\kappa x} + C_2 e^{i\kappa x}] e^{i\omega t} \tag{1}$$

where $U(x)$ is the spatial amplitude distribution along x, and $q(t)$ is its time variation. Eq. (1) describes the vibration as two traveling waves, having the same wavelength, traveling in opposite directions along the structure. C_1, C_2 are complex constants, representing the different amplitudes and phase shift of the two traveling waves. The wavelength is defined as:

$$\lambda = \frac{2\pi}{\kappa} \tag{2}$$

Eq. (1) can also be realized as a composition of a standing wave and a traveling wave having the same wavelength [17]. It is possible to quantify the ratio between the traveling wave and the standing wave in this form by a scalar measure, often referred to as the Standing Wave Ratio (SWR). This measure determines how far is the vibration state, (according to its coefficients, C_1, C_2), from a pure traveling or standing wave. The SWR is defined as [15,16]:

$$\mathrm{SWR} = \frac{|C_1| + |C_2|}{||C_1| - |C_2||} \tag{3}$$

The SWR value becomes unity when the traveling wave prevails completely (either $C_1 = 0$ or $C_2 = 0$) and its value reaches infinity for a pure standing wave ($|C_1| = |C_2|$). By defining:

$$\begin{aligned} C_{\min} &= \min\{|C_1|, |C_2|\} \\ C_{\max} &= \max\{|C_1|, |C_2|\} \end{aligned} \tag{4}$$

A different scalar function, with a similar interpretation, is introduced:

$$J = \frac{C_{\min}}{C_{\max}} \tag{5}$$

The function J measures the ratio between the waves traveling in opposite directions that appear in Eq. (1). The values of J lie between 0 and 1. For a pure standing wave, one obtains $J = 1$ and for a pure traveling wave—$J = 0$. This behavior of the function J makes it preferable for the optimization stage that is described below.

2.2. Fitting an ellipse to identify the wave coefficients from measurements

In Ref. [16], it is shown that the spatial amplitude of a single wavelength vibration (such as given in Eq. (1)) is:

$$U(x) = (\mathrm{Re}(C_1) + i\mathrm{Im}(C_1)) e^{-i\kappa x} + (\mathrm{Re}(C_2) + i\mathrm{Im}(C_2)) e^{i\kappa x} \tag{6}$$

This expression can be reordered with separate real and imaginary parts:

$$U(x) = [(\mathrm{Re}(C_1) + \mathrm{Re}(C_2))\cos(\kappa x) + (\mathrm{Im}(C_1) - \mathrm{Im}(C_2))\sin(\kappa x)] + \mathrm{i}[(\mathrm{Im}(C_1) + \mathrm{Im}(C_2))\cos(\kappa x) + (\mathrm{Re}(C_2) - \mathrm{Re}(C_1))\sin(\kappa x)] \quad (7)$$

Inspecting Eq. (7), it can be seen that it traces an ellipse in the complex plane [16,17]. This ellipse is characterized by its two radii r_1, r_2 from which the SWR can be computed. Measuring several points along the structure, it is possible to curve-fit an ellipse and to estimate its parameters. It was shown in Refs. [15–17] that the curve fitting procedure could be accomplished without an a priori knowledge of the wavenumber κ. Having fitted the ellipse, it is later possible to estimate the wavenumber as shown in Ref. [15].

Inspecting Eq. (7), it is possible to see that when the vibrations describe a pure standing wave (e.g. $C_1 = C_2$), the ellipse degenerates into a straight line. On the other hand, when the wave is a pure traveling wave (e.g. either $C_1 = 0$ or $C_2 = 0$), the ellipse becomes a pure circle. It is therefore possible to evaluate how the measured vibration state is close to a pure progressive wave by an expression that signifies how far the fitted ellipse from a pure circle is. This process can be carried out by defining a scalar value:

$$J = \frac{|r_1 - r_2|}{r_1 + r_2} \quad (8)$$

One can verify that the former definition of J is identical to the previously defined function given in Eq. (5), but it is based on the estimated radii of the ellipse that can be extracted from the measured response.

In the case where additional wavelengths exist in the spatial vibration, the complex representation of the spatial vibrations is composed of a sum of several ellipses which does no longer sum to a single ellipse. Curve fitting a linear model, in this case is impossible without the prior knowledge of the involved wavelengths. The ESPRIT algorithm overcomes this limitation, as described below.

2.3. Using ESPRIT to identify waves having several wavelengths

This section provides a brief introduction to the ESPRIT algorithm and its adaptation to spatial wave identification. A detailed description of the basic algorithm can be found in Refs. [19,20]. The ESPRIT algorithm was proposed to estimate the frequencies of a set of complex exponentials with added noise. This is completely equivalent to finding traveling wave components of a spatial signal. A spatial response consisting of N exponentials with different wavenumbers $\kappa_1, \ldots, \kappa_N$ and additive noise is described by:

$$y(x) = \sum_{p=1}^{N} \alpha_p \, \mathrm{e}^{\mathrm{i}\kappa_p x} + \mathrm{e}(x) \quad (9)$$

where $\mathrm{e}(x)$ is a zero-mean white Gaussian noise with mean square value of σ^2. The spatial response is captured by an array of m equally spaced sensors, located at $x_1, \ldots, x_m$. The array is partitioned into two sub-arrays, that are displaced in space with respect to each other. The first sub-array contains the sensors located at $x_1, \ldots, x_{m-1}$ while the second contains the sensors located at $x_2, \ldots, x_m$. Based on the parametric model given in Eq. (9), the transformation, $\mathbf{T}$, from one sub-array readings into the other one is [20]:

$$\mathbf{T} = \begin{bmatrix} \mathrm{e}^{-\mathrm{i}\kappa_1} & & \\ & \ddots & \\ & & \mathrm{e}^{-\mathrm{i}\kappa_N} \end{bmatrix} \quad (10)$$

This transformation performs a rotation in the complex plane or a shift in space. The ESPRIT seeks to identify this transformation from which the wavenumbers can be evaluated.

Both signal and noise subspaces are spanned by the covariance matrix, $\mathbf{R}$. Calculating the covariance matrix of $y(x)$ over m sensors [20]:

$$R = E[\, y(x) \quad y^H(x) \,] \quad (11)$$

and computing the singular value decomposition of **R** (SVD), one has:

$$\mathbf{R} = \mathbf{U}\mathbf{D}\mathbf{V}^H \tag{12}$$

It is assumed that the N largest singular values belong to the signal space so it can be separated from the noise space. The corresponding N columns of **U** span the signal space. The signal space is partitioned in the same manner as the sensor array; let $\mathbf{S}_1$, $\mathbf{S}_2$ be the signal spaces from the $m-1$ foremost and latter sensors. Obviously, both $\mathbf{S}_1$ and $\mathbf{S}_2$ span the same signal space, hence, there exists a transformation, $\boldsymbol{\varphi}$, between the two subspaces:

$$\mathbf{S}_1 = \boldsymbol{\varphi}\mathbf{S}_2 \tag{13}$$

It is shown that both $\boldsymbol{\varphi}$ and **T** share the same eigenvalues [20]. Thus, knowing $\boldsymbol{\varphi}$ enables one to calculate the wavenumbers. It is possible to estimate this transformation by solving Eq. (13) (in the least squares (LS) sense) by performing a pseudo inverse:

$$\hat{\boldsymbol{\varphi}} = \mathbf{S}_1\mathbf{S}_2^{+} \tag{14}$$

Having computed the transformation, the wavenumbers can be calculated via:

$$\kappa = -\arg(\mathrm{eig}(\hat{\boldsymbol{\varphi}})) \tag{15}$$

The dimension of the signal space, N, (being the number of expected wavenumbers) is related to the number of excitation frequencies (spectral lines). For each excitation frequency, it is anticipated to obtain, at least, a pair of wavenumbers—a positive one and a negative one. When more wavenumbers are expected (due to non-linear effects for example) N must be estimated separately.

Having estimated the wavenumbers, it is possible to calculate the waves' coefficients $\alpha_1, \ldots, \alpha_N$ by employing a LS type of estimation to Eq. (9):

$$\begin{bmatrix} y(x_1) \\ \vdots \\ y(x_m) \end{bmatrix} = \begin{bmatrix} e^{i\kappa_1 x_1} & \cdots & e^{i\kappa_N x_1} \\ \vdots & & \vdots \\ e^{i\kappa_1 x_m} & \cdots & e^{i\kappa_N x_m} \end{bmatrix} \begin{bmatrix} \alpha_1 \\ \vdots \\ \alpha_N \end{bmatrix} \tag{16}$$

Being complex, the wave coefficients, $\alpha_1, \ldots, \alpha_N$, represent the different wave amplitude and phase shifts. Eq. (16) has a unique solution only when $m \geqslant N$, i.e. the number of sensors is greater or equal to the number of identified waves. This is a basic requirement in the ESPRIT, otherwise it is not possible to separate between the signal and noise spaces.

For each frequency of vibration, a term in the form of Eq. (1) is added to the signal's parametric model; where one should expect to obtain, from the ESPRIT, a pair of wavenumbers—$\pm\kappa$. The ESPRIT algorithm can thus curve-fit waves with multiple wavelengths and these waves can be decomposed into their traveling and standing parts.

3. Traveling waves in a one-dimensional structures

This section discusses the generation of traveling waves in a finite structure from a theoretical point of view. The active sink method is presented and applied to a taut vibrating string. The necessary excitation forces to obtain a pure traveling wave in the string are then calculated and the results are discussed. The influence of the boundaries and, the uncertainties in the model on the traveling wave properties is examined. The analysis shows that the theoretical calculations are not useful in practical structures for the purpose of creating pure traveling waves.

3.1. Generating traveling waves in a string

Considering the string illustrated in Fig. 1, the properties and boundary conditions are outlined below. The string has a length L, cross area section A, thickness h, and volume density ρ. The string experiences a tension force T. Its boundaries are modeled by two masses m_{za}, m_{zb} and two springs k_{za}, k_{zb} where $z = 1$ denote the string's left edge and $z = 2$ denotes the right edge. The active sink method uses two active forces to generate traveling waves along the string. One force acts as a source, pumping energy into the string, while the other is

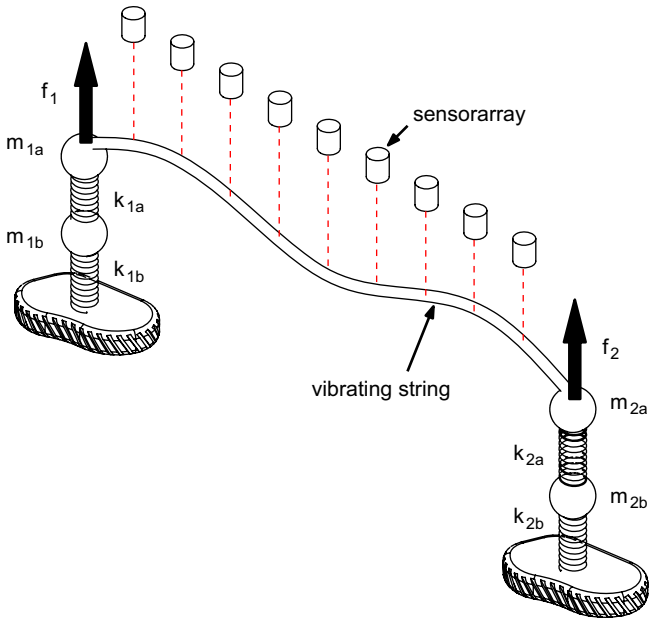

Fig. 1. Schematics of a string on flexible supports, excited by two forces applied at the edges.

the sink, absorbing the incoming waves. The forces f_1, f_2 are applied at the string edges affecting its boundaries. The string's deflection is denoted $u(x,t)$ and the point masses, m_{1b}, m_{2b} move according to two additional generalized coordinates, y_1, y_2, respectively. The string's equation of motion is described by the one-dimensional wave equation [23]:

$$\rho A\frac{\partial^2 u}{\partial t^2}-T\frac{\partial^2 u}{\partial x^2}=0 \tag{17}$$

The boundary conditions that incorporate the external harmonic forces:

$$\begin{aligned}
T\frac{\partial u}{\partial x}\bigg|_{x=0} &= -f_1\,\mathrm{e}^{\mathrm{i}\omega t}+m_{1a}\frac{\partial^2 u}{\partial t^2}\bigg|_{x=0}+k_{1a}(u|_{x=0}-y_1)\\
T\frac{\partial u}{\partial x}\bigg|_{x=L} &= f_2\,\mathrm{e}^{\mathrm{i}\omega t}-m_{2a}\frac{\partial^2 u}{\partial t^2}\bigg|_{x=L}-k_{2a}(u|_{x=L}-y_2)\\
m_{1b}\ddot{y}_1 &= k_{1a}(u|_{x=0}-y_1)-k_{1b}y_1\\
m_{2b}\ddot{y}_2 &= k_{2a}(u|_{x=L}-y_2)-k_{2b}y_2
\end{aligned} \tag{18}$$

It proves useful to define some standard and normalized parameters. The wave velocity is defined as:

$$c=\sqrt{\frac{T}{\rho A}} \tag{19}$$

It is possible to choose a non-dimensional space ordinate ξ such that:

$$\xi=\frac{x}{L} \tag{20}$$

and by defining:

$$\omega_0=\frac{c}{L} \tag{21}$$

A non-dimensional time, τ, is introduced:

$$\tau = \omega_0 t \tag{22}$$

The vibrations are normalized by the string's thickness h:

$$\begin{aligned} \tilde{u} &= \frac{u}{h} \\ \tilde{y}_r &= \frac{y_r}{h} \quad r = 1,2 \end{aligned} \tag{23}$$

It is now possible to rewrite Eqs. (17) and (18) in dimensionless equations:

$$\frac{\partial^2 \tilde{u}}{\partial \tau^2} - \frac{\partial^2 \tilde{u}}{\partial \xi^2} = 0 \tag{24}$$

The string's non-dimensional boundary conditions can now be expressed as:

$$\begin{aligned} \left.\frac{\partial \tilde{u}}{\partial \xi}\right|_{\xi=0} &= -F_1 \, e^{i\Omega\tau} + \mu_{1a} \left.\frac{\partial^2 \tilde{u}}{\partial \tau^2}\right|_{\xi=0} + \alpha_{1a}(\tilde{u}|_{\xi=0} - \tilde{y}_1) \\ \left.\frac{\partial \tilde{u}}{\partial \xi}\right|_{\xi=1} &= F_2 \, e^{i\Omega\tau} - \mu_{2a} \left.\frac{\partial^2 \tilde{u}}{\partial \tau^2}\right|_{\xi=1} - \alpha_{2a}(\tilde{u}|_{\xi=1} - \tilde{y}_2) \\ \mu_{1b}\ddot{\tilde{y}}_1 &= \alpha_{1a}(\tilde{u}|_{\xi=0} - \tilde{y}_1) - \alpha_{1b}\tilde{y}_1 \\ \mu_{2b}\ddot{\tilde{y}}_2 &= \alpha_{2a}(\tilde{u}|_{\xi=1} - \tilde{y}_2) - \alpha_{2b}\tilde{y}_2 \end{aligned} \tag{25}$$

where the following non-dimensional parameters are defined:

$$\begin{aligned} \alpha_{rz} &= \frac{k_{rz}L}{T}; \quad \mu_{rz} = \frac{m_{rz}}{\rho A L}, \quad z = a,b \\ F_r &= \frac{f_r L}{Th}, \quad r = 1,2 \\ \Omega &= \frac{\omega L}{c} \end{aligned} \tag{26}$$

A general solution for the string's vibrations under harmonic excitations is composed of two traveling waves, having the same wavelength but that travel in opposite directions:

$$\tilde{u}(\xi,\tau) = (C_1 \, e^{-i\kappa\xi} + C_2 \, e^{i\kappa\xi}) \, e^{i\Omega\tau} \tag{27}$$

where κ is the non-dimensional wavenumber:

$$\kappa = \frac{\omega}{c} L = \frac{\omega}{\omega_0} = \Omega, \tag{28}$$

and the general non-dimensional solution for the vibrations of m_{1b}, m_{2b} is given by:

$$\begin{aligned} \tilde{y}_1 &= C_3 \, e^{i\Omega\tau} \\ \tilde{y}_2 &= C_4 \, e^{i\Omega\tau} \end{aligned} \tag{29}$$

By substituting Eqs. (27) and (29) into Eq. (25), a linear set of equations $\mathbf{BC} = \mathbf{F}$ can be formed:

$$\underbrace{\begin{bmatrix} \mathbf{B}_1 & \mathbf{B}_2 \\ \mathbf{B}_3 & \mathbf{B}_4 \end{bmatrix}}_{\mathbf{B}} \underbrace{\begin{bmatrix} C_1 \\ C_2 \\ C_3 \\ C_4 \end{bmatrix}}_{\mathbf{C}} = \underbrace{\begin{bmatrix} F_1 \\ F_2 \\ 0 \\ 0 \end{bmatrix}}_{\mathbf{F}} \tag{30}$$

and:

$$\mathbf{B}_1 = \begin{bmatrix} \alpha_{1a} - \mu_{1a}\Omega^2 + \mathrm{i}\kappa & \alpha_{1a} - \mu_{1a}\Omega^2 - \mathrm{i}\kappa \\ (\alpha_{2a} - \mu_{2a}\Omega^2 - \mathrm{i}\kappa)\,\mathrm{e}^{-\mathrm{i}\kappa} & (\alpha_{2a} - \mu_{2a}\Omega^2 + \mathrm{i}\kappa)\,\mathrm{e}^{\mathrm{i}\kappa} \end{bmatrix}, \quad \mathbf{B}_2 = \begin{bmatrix} -\alpha_{1a} & 0 \\ 0 & -\alpha_{2a} \end{bmatrix}$$

$$\mathbf{B}_3 = \begin{bmatrix} -\alpha_{1a} & -\alpha_{1a} \\ -\alpha_{2a}\,\mathrm{e}^{-\mathrm{i}\kappa} & -\alpha_{2a}\,\mathrm{e}^{\mathrm{i}\kappa} \end{bmatrix}, \quad \mathbf{B}_4 = \begin{bmatrix} (\alpha_{1a} + \alpha_{1b}) - \mu_{1b}\Omega^2 & 0 \\ 0 & (\alpha_{2a} + \alpha_{2b}) - \mu_{2b}\Omega^2 \end{bmatrix} \tag{31}$$

The response can be calculated from Eq. (30) only when $\det(\mathbf{B}) \neq 0$, i.e. the string is not at resonance. When the string is excited at one of its natural frequencies, only a single mode is excited, this mode is a pure standing wave. In the former case it is not possible, theoretically, to excite a traveling wave as all the injected power is absorbed by one of the string's natural modes.

By algebraic manipulation of Eq. (30), it is possible to calculate the forces F_1, F_2 that generate any desired combination of the forward and backward traveling waves (i.e. imposing values for C_1, C_2):

$$\begin{bmatrix} F_1 \\ F_2 \end{bmatrix} = (\mathbf{B}_1 - \mathbf{B}_2\mathbf{B}_4^{-1}\mathbf{B}_3) \begin{bmatrix} C_1 \\ C_2 \end{bmatrix} \tag{32}$$

Having found the necessary forces, the vibrations of the masses at the edges can also be calculated:

$$\begin{bmatrix} C_3 \\ C_4 \end{bmatrix} = -\mathbf{B}_4^{-1}\mathbf{B}_3 \begin{bmatrix} C_1 \\ C_2 \end{bmatrix} \tag{33}$$

Eqs. (32) and (33) are valid as long as $\mathbf{B}_4$ is nonsingular, i.e. as long as none of the boundaries experiences a local resonance.

Specifically, when one seeks to generate a pure traveling wave (in the positive direction for example), with amplitude C_0, the wave coefficients are set to:

$$\begin{aligned} C_1 &= C_0 \\ C_2 &= 0 \end{aligned} \tag{34}$$

Substituting Eq. (34) into Eq. (32), the forces required to generate the desired traveling wave are:

$$\begin{bmatrix} F_1 \\ F_2 \end{bmatrix} = \begin{bmatrix} (\alpha_{1a} - \mu_{1a}\Omega^2 + \mathrm{i}\kappa) + \dfrac{\alpha_{1a}^2}{\alpha_{1a} + \alpha_{1b} - \mu_{1b}\Omega^2} \\ (\alpha_{2a} - \mu_{2a}\Omega^2 - \mathrm{i}\kappa)\,\mathrm{e}^{-i\kappa} - \dfrac{\alpha_{2a}^2\,\mathrm{e}^{-i\kappa}}{\alpha_{2a} + \alpha_{2b} - \mu_{2b}\Omega^2} \end{bmatrix} C_0. \tag{35}$$

And the vibrations of the non-dimensional edge masses μ_{1b}, μ_{2b} (see Fig. 1), in the case of a traveling wave, become:

$$\begin{bmatrix} C_3 \\ C_4 \end{bmatrix} = \begin{bmatrix} \dfrac{\alpha_{1a}}{\alpha_{1a} + \alpha_{1b} - \mu_{1b}\Omega^2} \\ \dfrac{\alpha_{2a}\,\mathrm{e}^{-i\kappa}}{\alpha_{2a} + \alpha_{2b} - \mu_{2b}\Omega^2} \end{bmatrix} C_0. \tag{36}$$

Sometimes it is more convenient to set one of the forces as a reference force rather than imposing the traveling wave amplitude. Setting F_1 as a reference force, the wave amplitude, C_0, may be calculated from Eq. (35):

$$C_0 = \left[(\alpha_{1a} - \mu_{1a}\Omega^2 + \mathrm{i}\kappa) + \frac{\alpha_{1a}^2}{\alpha_{1a} + \alpha_{1b} - \mu_{1b}\Omega^2} \right]^{-1} F_1 \tag{37}$$

It is now possible to use the second half of Eq. (35) with Eq. (37) and calculate the force ratio, F_2/F_1, needed to generate a pure traveling wave:

$$F_{\mathrm{RATIO}} = \frac{F_2}{F_1} = \frac{[(\alpha_{2a} - \mu_{2a}\Omega^2 - \mathrm{i}\kappa) - (\alpha_{2a}^2/(\alpha_{2a} + \alpha_{2b} - \mu_{2b}\Omega^2))]\,e^{-\mathrm{i}\kappa}}{(\alpha_{1a} - \mu_{1a}\Omega^2 + \mathrm{i}\kappa) + (\alpha_{1a}^2/(\alpha_{1a} + \alpha_{1b} - \mu_{1b}\Omega^2))} \tag{38}$$

Eq. (38) describes the amplitude ratio, $|F_{\mathrm{RATIO}}|$, and a phase shift, $\measuredangle F_{\mathrm{RATIO}}$, between the two edge-forces, these proportions generate a pure traveling wave in the positive direction of the string, as long as the system is modeled accurately. The amplitude of the desired wave is given in Eq. (37). In reality, the result of Eq. (38) is not useful due to the limitations in model accuracy. This is further elaborated next in Section 3.3.

3.2. The influence of boundary dynamics on the traveling wave solution

As reflected from the expressions given in Eqs. (35)–(38), the conditions under which a desired vibration pattern is generated, and in particular a traveling wave pattern, depend on the string's properties and on the dynamical model of the boundary supports. The effects of the properties and boundary conditions on the obtained traveling wave are analyzed in this section.

It proves convenient to study first the simplest case where the string is completely free:

$$\begin{aligned} &\alpha_{1a} = \alpha_{1b} = \alpha_{2a} = \alpha_{2b} = 0 \\ &\mu_{1a} = \mu_{2a} = 0 \end{aligned} \tag{39}$$

In this case, the force ratio (from Eq. (38)) becomes:

$$F_{\mathrm{RATIO}} = -\mathrm{e}^{-\mathrm{i}\kappa} \tag{40}$$

This ratio depends only on the properties of the string and it represents a pure phase shift between the two forces. The phase shift is related to the time of flight of a disturbance from one edge of the string to the other.

Another interesting case is the case of symmetric boundaries (the right and left boundaries are identical):

$$\begin{aligned} &\alpha_{1a} = \alpha_{2a} \triangleq \alpha_a, \quad \alpha_{1b} = \alpha_{2b} \triangleq \alpha_b \\ &\mu_{1a} = \mu_{2a} \triangleq \mu_a, \quad \mu_{1b} = \mu_{2b} \triangleq \mu_b \end{aligned} \tag{41}$$

The force ratio for the symmetric boundary conditions (from Eq. (38)) is:

$$F_{\mathrm{RATIO}} = \mathrm{e}^{-\mathrm{i}\kappa} \frac{(\alpha_a - \mu_a\Omega^2)(\alpha_a + \alpha_b - \mu_b\Omega^2) - \alpha_a^2 - \mathrm{i}\kappa(\alpha_a + \alpha_b - \mu_b\Omega^2)}{(\alpha_a - \mu_a\Omega^2)(\alpha_a + \alpha_b - \mu_b\Omega^2) - \alpha_a^2 + \mathrm{i}\kappa(\alpha_a + \alpha_b - \mu_b\Omega^2)} \tag{42}$$

It is possible to see that, in this case, $|F_{\mathrm{RATIO}}| = 1$ and the phase lag depends on the mass, stiffness, and geometrical parameters. This means that for a pure symmetric system, only the phase between the two forces has to be set to obtain the desired traveling wave response.

In order to clarify the role of the boundary conditions, a simpler case is inspected. In this example, the force F_1 is applied at a free edge of the string and the force F_2 is applied at an edge whose boundary consists of a mass and two identical springs. The non-dimensional boundary parameters in this case are:

$$\begin{aligned} &\alpha_{1a} = \alpha_{1b} = 0, \quad \mu_{1a} = \mu_{2a} = 0 \\ &\alpha_{2a} = \alpha_{2b} \triangleq \alpha_2, \quad \mu_{2b} \neq 0 \end{aligned} \tag{43}$$

Eqs. (30) and (31) degenerate into:

$$\begin{bmatrix} \mathrm{i}\kappa & -\mathrm{i}\kappa & 0 \\ (\alpha_2 - \mathrm{i}\kappa)\,\mathrm{e}^{-\mathrm{i}\kappa} & (\alpha_2 + \mathrm{i}\kappa)\,\mathrm{e}^{\mathrm{i}\kappa} & -\alpha_2 \\ -\alpha_2\,\mathrm{e}^{-\mathrm{i}\kappa} & -\alpha_2\,\mathrm{e}^{\mathrm{i}\kappa} & (2\alpha_2 - \mu_{2b}\Omega^2) \end{bmatrix} \begin{bmatrix} C_1 \\ C_2 \\ C_4 \end{bmatrix} = \begin{bmatrix} F_1 \\ F_2 \\ 0 \end{bmatrix} \tag{44}$$

and the force ratio (from Eq. (38)) becomes:

$$F_{\mathrm{RATIO}} = -\mathrm{e}^{-\mathrm{i}\kappa}\left[1 + \frac{\mathrm{i}\alpha_2}{\kappa}\frac{\alpha_2 - \mu_{2b}\Omega^2}{2\alpha_2 - \mu_{2b}\Omega^2}\right] \tag{45}$$

It can be seen from Eq. (45) that the dynamics of the boundary have a considerable effect on the force ratio that creates a pure traveling wave.

Two special excitation frequency values are examined. The first excitation frequency of interest is:

$$\Omega = \sqrt{\frac{\alpha_2}{\mu_{2b}}} \tag{46}$$

For this frequency, the force ratio degenerates back to Eq. (40) of the free–free string and the amplitude of vibration of the mass μ_{2b} is:

$$C_4 = C_0 \, \mathrm{e}^{-\mathrm{i}\kappa} \tag{47}$$

The mass μ_{2b} vibrates at the same amplitude and in-phase with the string edge. Thus, the boundary dynamics have no effect on the string dynamics.

The second frequency of excitation of interest is:

$$\Omega = \sqrt{\frac{2\alpha_2}{\mu_{2b}}} \tag{48}$$

In this frequency:

$$\begin{aligned} F_{\mathrm{RATIO}} &\to \infty \\ C_4 &\to \infty \end{aligned} \tag{49}$$

This frequency is the natural frequency of the sub-system composed of the mass μ_{2b} with the two springs α_{2a}, α_{2b} fixed at the upper side of α_{2a}. This means that when the supporting system is at resonance (locally), it acts as a dynamic mass-absorber and no finite amplitude of F_2 can generate a sufficient amount of energy to create a traveling wave having finite amplitude. All the energy injected by F_1 goes to the vibration of the mass μ_{2b} rather than to the string's vibration. A realistic boundary would have an infinite number of (local) natural frequencies and modes. When one of the boundary's local modes is excited, the generation of a traveling wave becomes a demanding task in terms of the power consumption.

It is also possible to verify that there is no real value of the excitation frequency, Ω, that renders the force ratio zero. This is due to the fact that it is not possible to match the resistive characteristic impedance of the string by using only energy conserving elements.

3.3. Sensitivity of the traveling wave conditions to modeling uncertainties

The model of the structure has limited accuracy and it contains some uncertainty in its parameters. In the case of the string, uncertainties in the string's tension, density and dimensions are expected. In addition, in the current string model the damping effect is unaccounted for, while in reality some dissipation always exists. Moreover the stiffness and masses at the boundary supports are a simplification of true supports and therefore are imperfect. When applying the forces based on the theoretical model, it is unlikely that pure traveling waves will be formed.

In order to assess the importance of each physical parameter, i.e. stiffness, mass, damping and frequency on the ability to form traveling waves, these quantities are varied mathematically and the effect is examined.

The non-dimensional parameter κ represents the string properties and the non-dimensional parameters α_2, μ_{2b}, reflect the boundary conditions. Let a nominal model having the nominal parameters κ^0, α_2^0, μ_{2b}^0 and let F_1^0, F_2^0 be the forces that generate a pure traveling wave according to Eq. (45) (i.e. for a nominal model). It is possible to investigate the response of a perturbed model of the string when applying the nominal forces F_1^0, F_2^0, by perturbing Eq. (44) and calculating the string's response. Since the force ratio is a complex value, it reflects an amplitude ratio and a phase shift between the two forces; the perturbation s hould be done in both amplitudes and phases of the parameters. The meaning of imaginary perturbation to a real parameter is interpreted as adding structural damping to the model. The perturbed string's

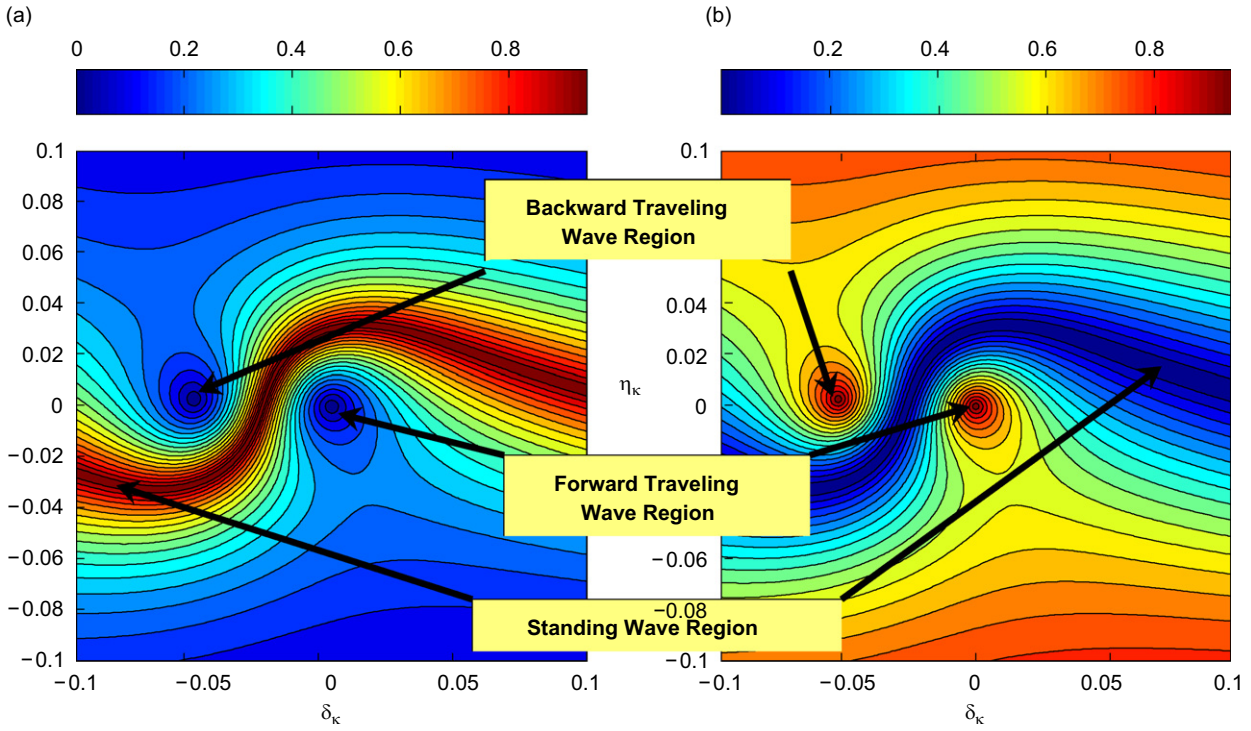

Fig. 2. The effect of perturbing the non-dimensional wavenumber, κ, on the traveling wave as reflected by: (a) the value of $J(\delta_\kappa, \eta_\kappa)$; (b) the value of $\mathrm{SWR}^{-1}(\delta_\kappa, \eta_\kappa)$.

parameters are thus:

$$\begin{aligned}\tilde{\kappa} &= \kappa^0(1+\delta_\kappa)\,\mathrm{e}^{\mathrm{i}\eta_\kappa}\\ \tilde{\alpha}_2 &= \alpha_2^0(1+\delta_{\alpha_2})\,\mathrm{e}^{\mathrm{i}\eta_{\alpha_2}}\\ \tilde{\mu}_{2b} &= \mu_{2b}^0(1+\delta_{\mu_{2b}})\,\mathrm{e}^{\mathrm{i}\eta_{\mu_{2b}}}\end{aligned} \tag{50}$$

where δ_p, η_p are amplitude and phase perturbation in the parameter p, respectively. The degree of purity of the resulting wave is obtained by calculating the wave coefficients, C_1, C_2, from Eq. (44):

$$\begin{bmatrix} C_1 \\ C_2 \\ C_4 \end{bmatrix} = \begin{bmatrix} \mathrm{i}\tilde{\kappa} & -\mathrm{i}\tilde{\kappa} & 0 \\ (\tilde{\alpha}_2 - \mathrm{i}\tilde{\kappa})\,\mathrm{e}^{-\mathrm{i}\kappa} & (\tilde{\alpha}_2 + \mathrm{i}\tilde{\kappa})\,\mathrm{e}^{\mathrm{i}\kappa} & -\tilde{\alpha}_2 \\ -\tilde{\alpha}_2\,\mathrm{e}^{-\mathrm{i}\tilde{\kappa}} & -\tilde{\alpha}_2\,\mathrm{e}^{\mathrm{i}\tilde{\kappa}} & (2\tilde{\alpha}_2 - \tilde{\mu}_{2b}\Omega^2) \end{bmatrix}^{-1} \begin{bmatrix} F_1^0 \\ F_2^0 \\ 0 \end{bmatrix} \tag{51}$$

and evaluating the SWR and J functions for various excitation frequencies (Ω). In Figs. 2 and 3, a few sample results are shown. The results are presented by the values of the J function—where 0 means a traveling wave and 1 is obtained for a standing wave (see Eq. (5)) and by the values of the SWR^{-1} function—0 means a standing wave and 1 is a traveling wave (see Eq. (3)).

In Fig. 2, the fluctuations of the values of the SWR^{-1} and J functions for perturbations of the string properties are presented for a normalized wavelength $\lambda = 0.3$. It can be seen that for a small variation in the parameter, the applied forces fails to generate the desired traveling wave. A region of a pure standing wave is noted for small perturbations. For example, reducing the value of κ to 95% of the nominal value renders the structure response to a standing wave solution. Another interesting point, as can be seen in Fig. 2, is that two regions where pure traveling waves exist are separated by a "valley" of standing waves. The difference between the two regions is the direction the waves travel. This information is not shown in the SWR function. In addition, it is evident that both SWR^{-1} and J functions hold the same information regarding the purity of waves in the response.

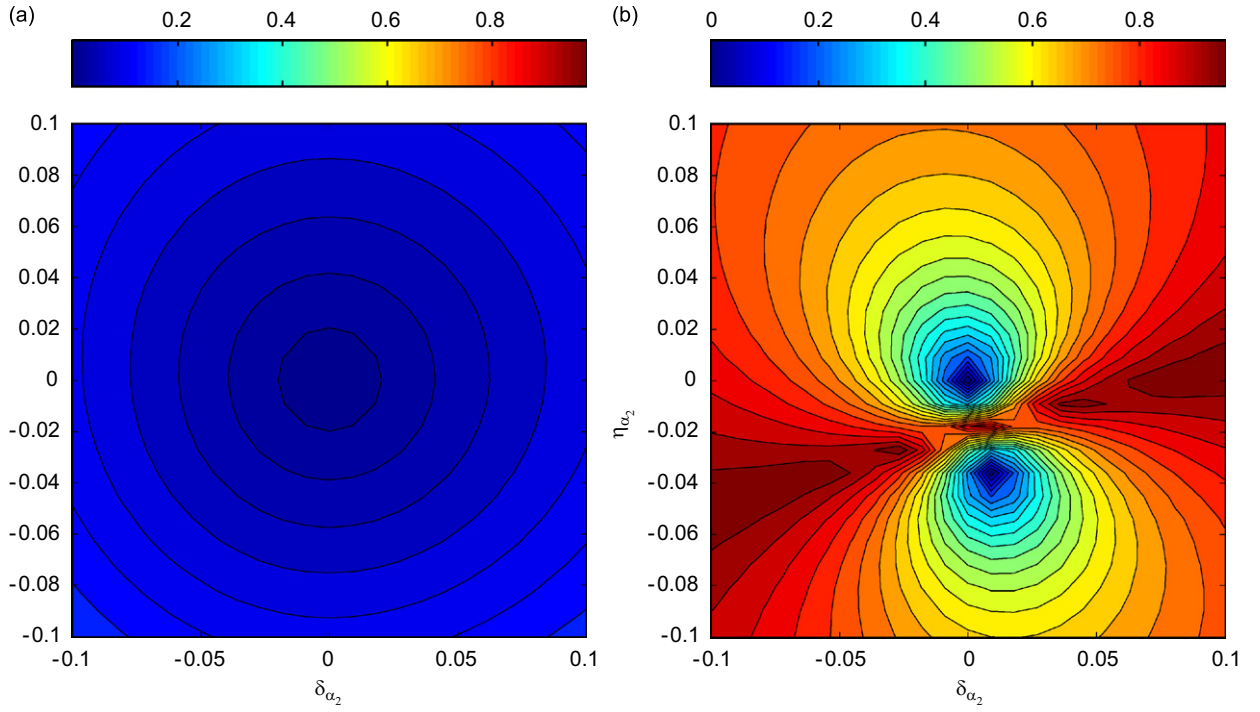

Fig. 3. The effect of perturbing the non-dimensional stiffness, α_2, on the traveling wave, as reflected by the value of $J(\delta_\kappa, \eta_\kappa)$. The non-dimensional excitation frequency is: (a) far from the critical frequency $\Omega \gg \sqrt{2\alpha_2/\mu_{2b}}$ ($\lambda = 0.3$) and (b) in the vicinity of the critical frequency $\Omega \approx \sqrt{2\alpha_2/\mu_{2b}}$ ($\lambda = 0.07$).

In Fig. 3(a), the fluctuations of the values of the J function for perturbations in the non-dimensional boundary stiffness α_2 are presented for $\lambda = 0.3$. Here, small changes in the stiffness cause only small changes in the forces needed to generate a traveling wave. Repeating this analysis for $\lambda = 0.07$, a value very close to the critical value of $\Omega \approx \sqrt{2\alpha_2/\mu_{2b}}$ (described in the previous section in Eq. (48)), is presented in Fig. 3(b). In this case, the sensitivity of the response to the perturbation is considerably higher and a very small uncertainty in the stiffness value or a little damping variation changes the traveling wave solution dramatically. Alternatively, a small modification of the stiffness would correct a problematic system with which it is difficult to generate traveling waves at a particular frequency. Similar results are obtained when perturbing the boundary mass μ_{2b}.

The actual force ratio needed to excite a desired response in a structure cannot be computed from a theoretical model or numerical model since small deviations can change the response significantly. The difference between the truly required forces and the theoretical ones can be fairly large in certain cases when the boundary plays an important role.

4. Tuning traveling waves in practice

As discussed in the previous section, it is not feasible to generate a pure traveling wave in a structure when only its theoretical model is considered. An experiment driven tuning process is suggested here. The tuning process is based on modifying the amplitude ratio and phase lag between the forces acting on the edges, and evaluating the resulting wave state of the structure by performing spatial measurements. The ratio between the forces is expressed as a complex value:

$$\frac{F_2}{F_1} = A_r \, e^{i\phi} \tag{52}$$

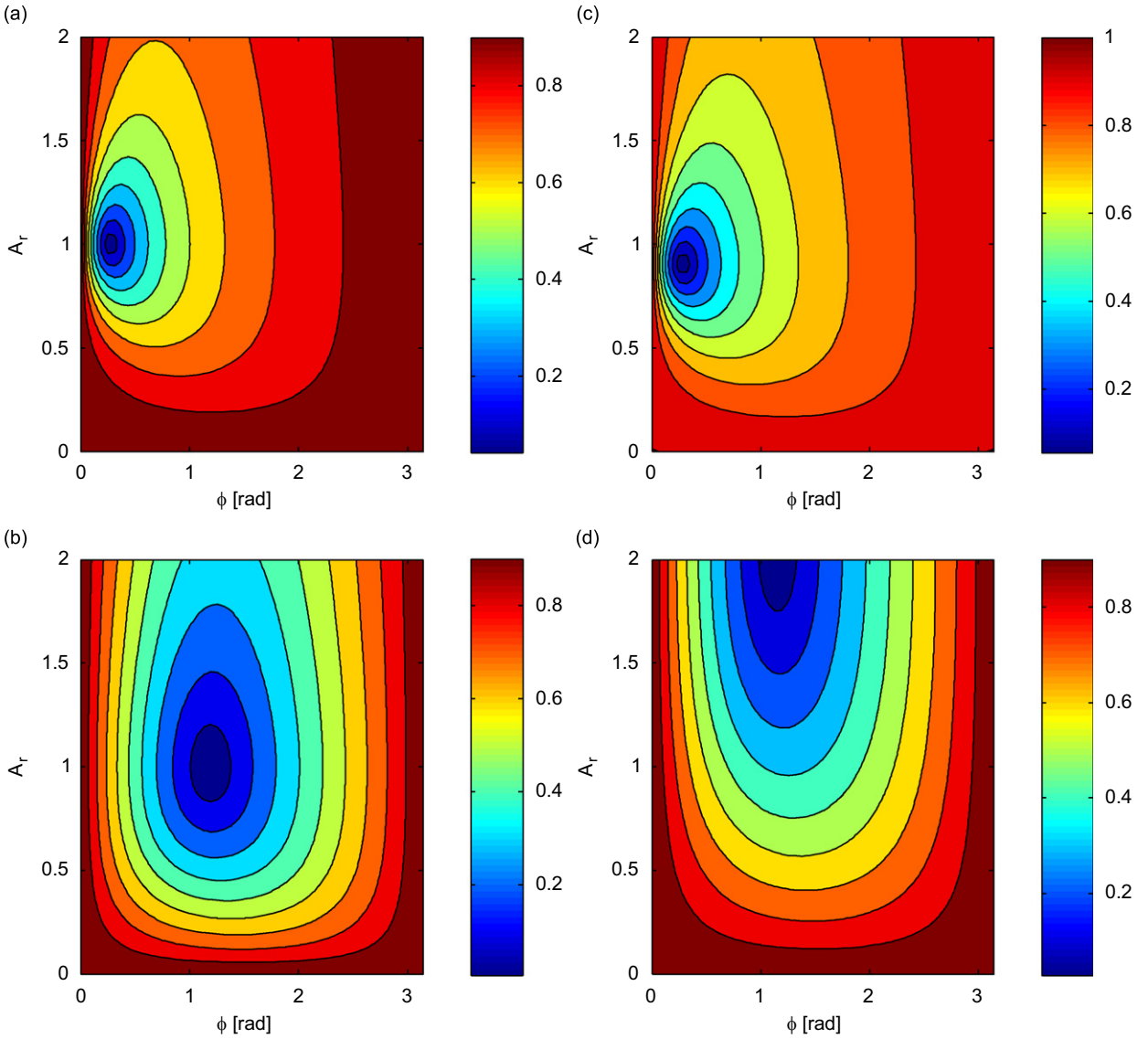

Fig. 4. Theoretical mapping of $J(\phi, A_r)$, over the phase shift and amplitude ratio domain, for various wavelengths and boundary conditions.

where A_r is an amplitude ratio and ϕ is a phase lag. The ratio of standing to traveling waves, is affected by the pair A_r, ϕ, and it is given by the SWR and/or J functions (both described in Section 2). The parameters A_r, ϕ are iteratively modified by the tuning process, until a desired level of purity of the traveling wave is achieved. The tuning process is described below in Section 4.2.

4.1. Mapping the phase and amplitude and their effect on traveling waves

As shown in Ref. [15], for a given excitation frequency, the function J can be mapped over the A_r, ϕ domain. Some observations regarding the map topology are discussed in Ref. [15] where it is noteworthy to mention the smoothness of the map in the A_r, ϕ domain, and also it is noticeable that the amplitude ratio and phase lag are nearly decoupled.

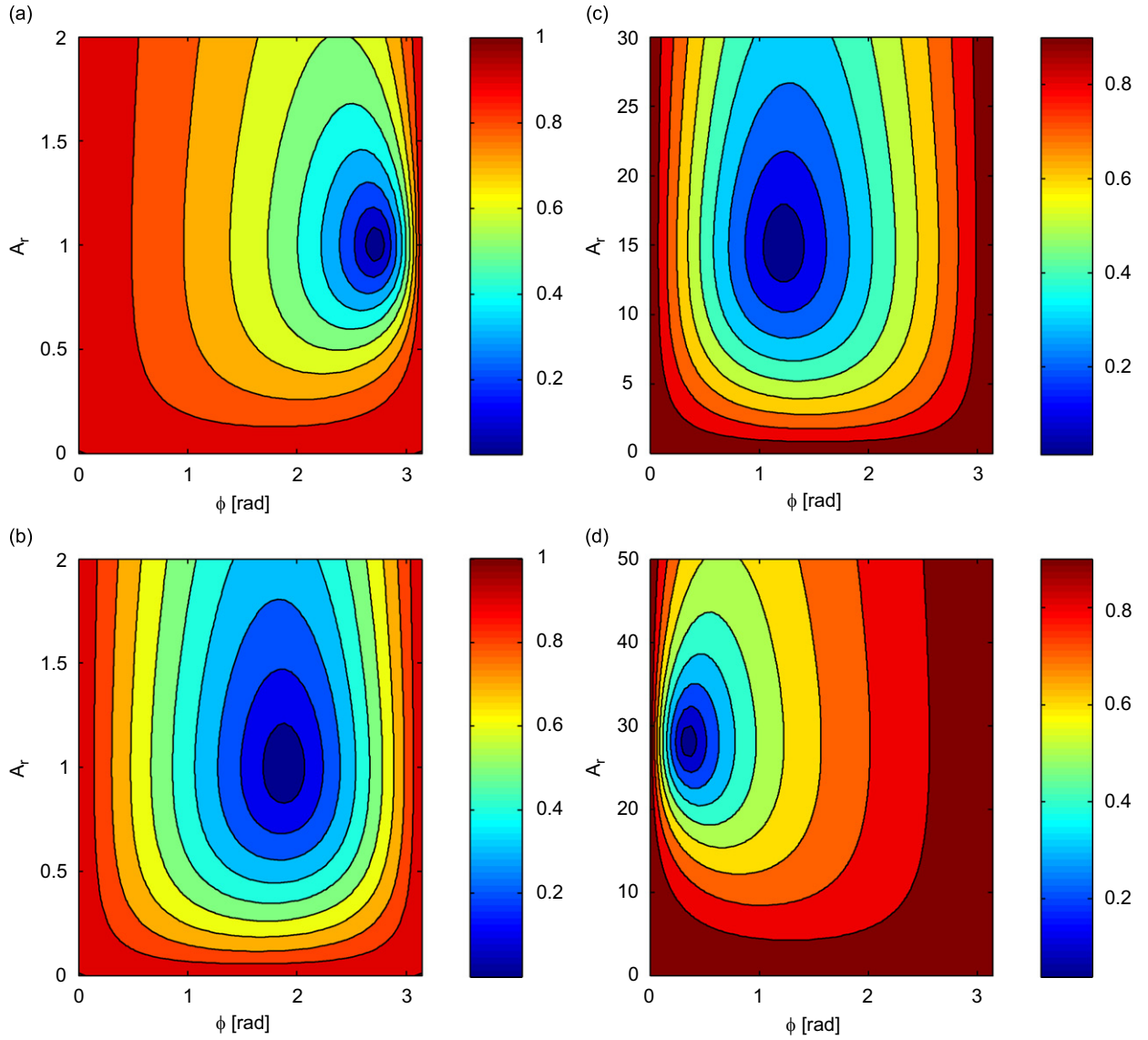

Fig. 5. Theoretical mapping of $J(\phi, A_r)$, over the phase shift and amplitude ratio domain, for various wavelengths and boundary conditions.

In Fig. 4, the maps for a string with symmetric boundaries (such as given in Eq. (41)) are shown alongside with the maps of the same string with slightly non-symmetric boundaries. As expected, for a string with symmetric boundary conditions, the force ratio is unity. While for different excitation frequencies only the phase between the two actuators has to be changed to maintain traveling waves (Fig. 4(a) and (b)). A slight deviation from the symmetric boundaries changes the map. Far from the critical excitation frequency (Eq. (48)), the amplitude ratio and phase lag changes are minor (Fig. 4(c)) while in the vicinity of the critical frequency the required change in the amplitude ratio is significant.

In Fig. 5, another set of maps is provided for comparison. The theoretical map for a string with free boundaries (described in Eq. (39)) is shown in Fig. 5(a) and (b). Once again, the force's amplitude ratio is unity due to the symmetry. A map for a string with one free edge (described in Eq. (43)) is given in Fig. 5(c) and (d). Here the forces' amplitude ratio is far from unity due to the asymmetry of the boundaries.

The preceding analysis has demonstrated that a slight deviation from the model of boundary conditions can yield a significant change in the required excitation amplitude that generates traveling waves. This emphasizes the need for an experimental force tuning stage.

4.2. Tuning via optimization

The tuning of traveling waves is a dual stage process. Initially, the structure's response is measured and decomposed into the traveling and standing components. It is possible now to evaluate the current wave state by calculating the value of the SWR and J (Eqs. (3) and (5)) of the measured response. Based on the estimated SWR, the algorithm modifies the amplitude ratio and phase of the external forces in order to optimize the value of the SWR/J functions toward a pure traveling wave state. The typically smooth topology of $J(\phi, A_r)$ makes it ideal as a target optimization function. By locating its minima, the force ratio generating the pure traveling wave for the structure is obtained. When the desired pattern contains more than one wavelength, an independent function $J_\lambda(\phi, A_r)$ exists for each wavelength, λ. An augmented cost function can be formulated:

$$J_a = \sum_n J_{\lambda_n}(\phi_n, A_{rn}) \tag{53}$$

Assuming that the measured response is a superposition of different excitation frequencies, the optimization can be carried out in the same manner as with a single wavelength. Now, n sets of amplitude and phase ratios are tuned simultaneously, in each iteration.

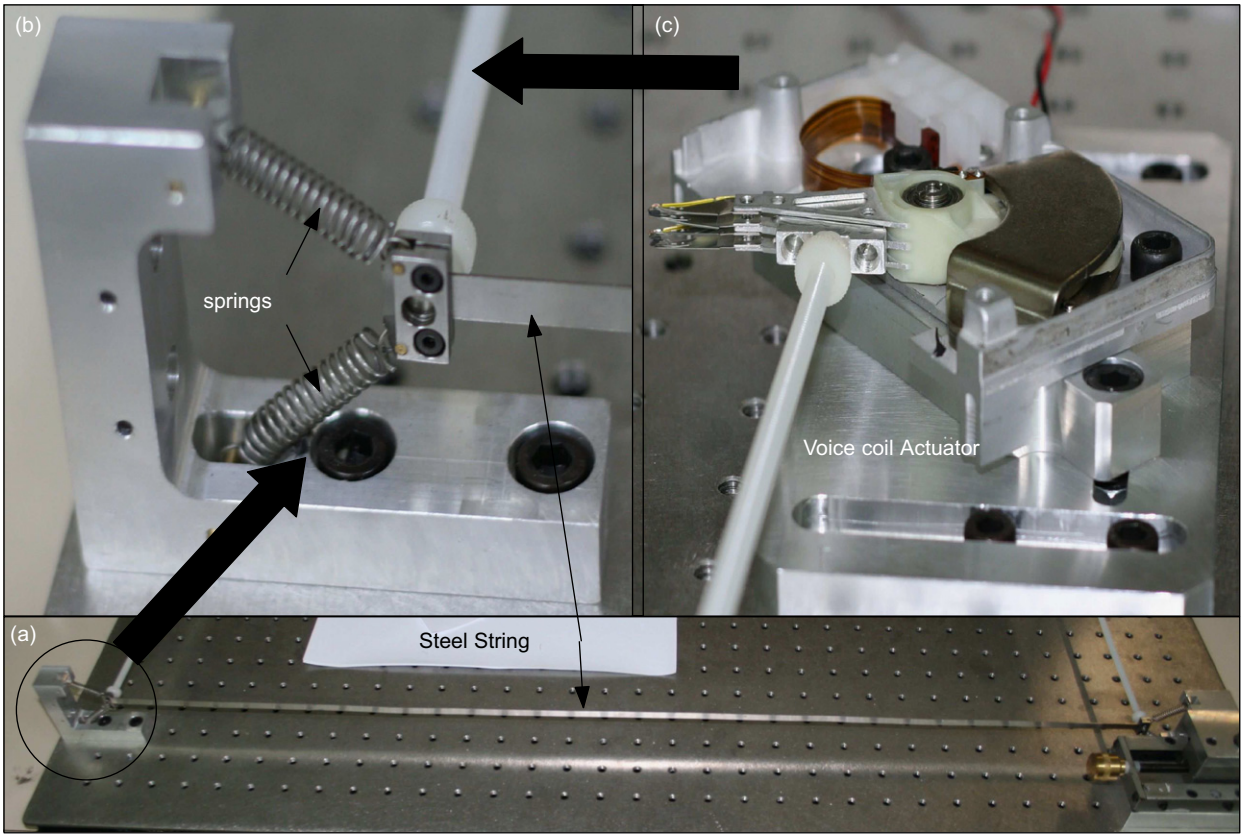

Fig. 6. Picture of the experimental system: (a) full view of the system, (b) a magnification of the left boundary and (c) a magnification of the voice-coil actuator.

5. Experimental verification

This section describes the experimental system and the series of experiments that were carried out to verify the one dimensional traveling waves generation and identification algorithm. The experimental system is depicted in Fig. 6. The system consists of a taut steel string of length $L = 0.77\,\mathrm{m}$ and a cross section of $A = 6 \times 0.5\,\mathrm{mm}^2$. The string is held by two adjustable springs (as shown in Fig. 6(b)). The excitation is realized by means of two voice-coil actuators, applying perpendicular forces to the string edges, as shown in Fig. 6(c). The voice-coils are powered by two current amplifiers that reduce the cross-coupling between the forces produced by the actuators. Measurements were taken using a scanning laser vibrometer (Polytec^{TM}) and all the data acquisition and calculations were performed via Matlab®. The excitation was produced by a dSPACE® system and measurements were collected by an Agilent E1433B multi-channel measurement system. The system exhibits imperfect connections between the actuators and the string with some inherent angular movement of the actuators that affects the string's edge response. To avoid these affects, the string's

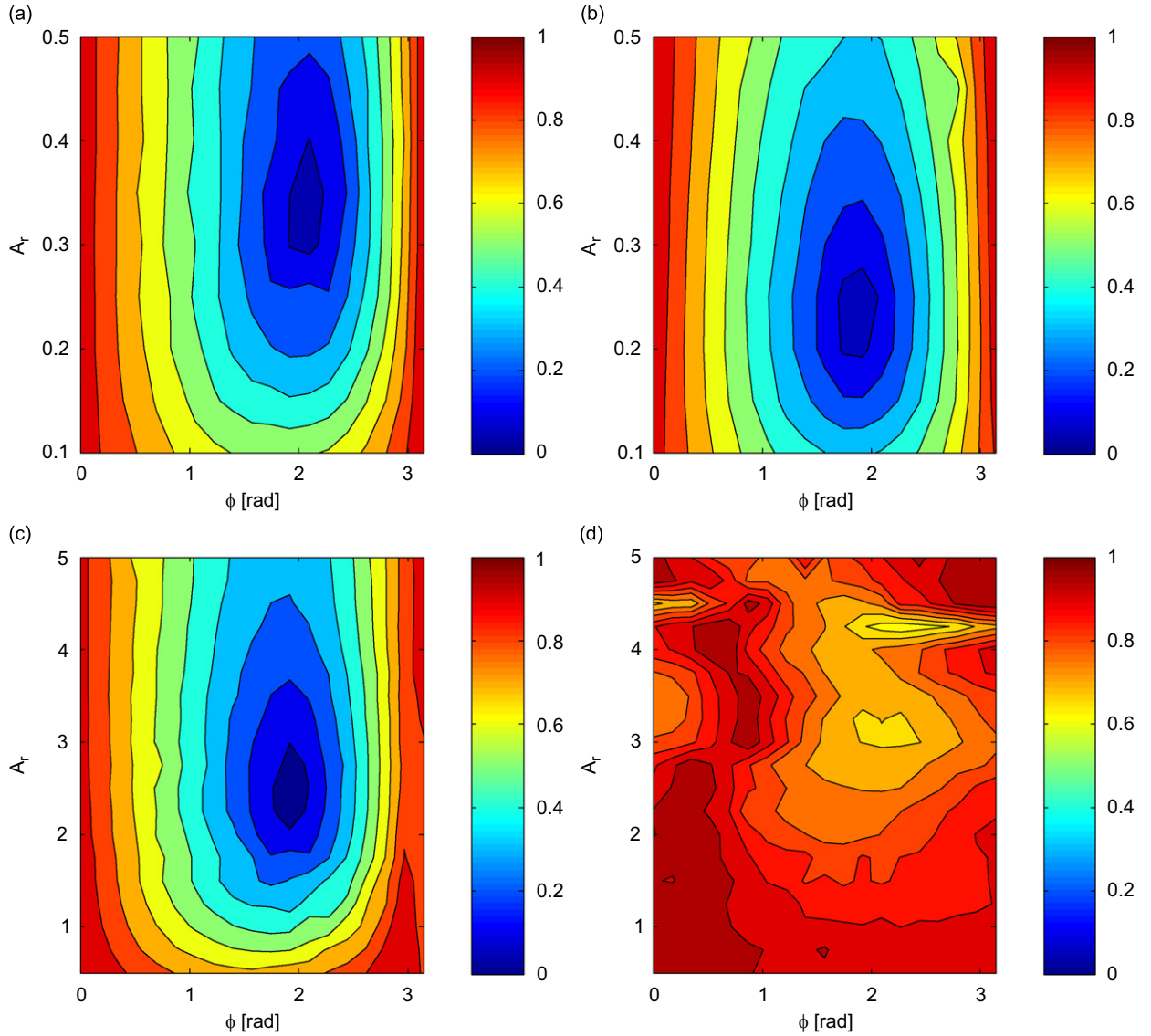

Fig. 7. Experimental maps of $J(\phi, A_r)$, over the phase shift and amplitude ratio domain, measured for several excitation frequencies: (a) $f = 76\,\mathrm{Hz}$; (b) $f = 95\,\mathrm{Hz}$; (c) $f = 235\,\mathrm{Hz}$ and (d) $f = 353\,\mathrm{Hz}$.

response was measured along the central region of the string (about 70% of its full length). The wave identification and tuning were carried out based on this measured region only.

The string's response to sinusoidal forces was measured at equally spaced points along the string. By curve fitting a harmonic function to the laser's measured signal at each point, the amplitude and relative phase are calculated. The phase is computed relative to one of the actuators signals. The amplitudes and phases of every point, along the string, form the spatial response of the string. This response is the input to the identification stage where the ESPRIT algorithm estimates the wavenumbers followed by estimating the wave coefficients as described in Section 2. According to the wave coefficients the cost function can be evaluated as an input to the tuning stage.

5.1. Measuring the cost function

The map of the function $J(\phi, A_r)$ for various excitation frequencies shows the feasibility of creating traveling waves via minimization of $J(\phi, A_r)$ for the experimental system. In Fig. 7, measured maps for several excitation frequencies are shown. Several observations can be made from the experimentally obtained maps. (i) The amplitude ratio is far from unity for all maps. This may suggest that the string and boundaries are not symmetric although they are designed to be so. (ii) It can be seen that the amplitude ratio and phase are nearly decoupled in practice. Thus, a local minimum can be achieved by varying only one of the parameters at a time (i.e. amplitude change followed by tuning the phase). (iii) Fig. 7(a) shows the map related to the frequency of 76 Hz. This map can be compared to the theoretical map calculated based on the system's parameters and

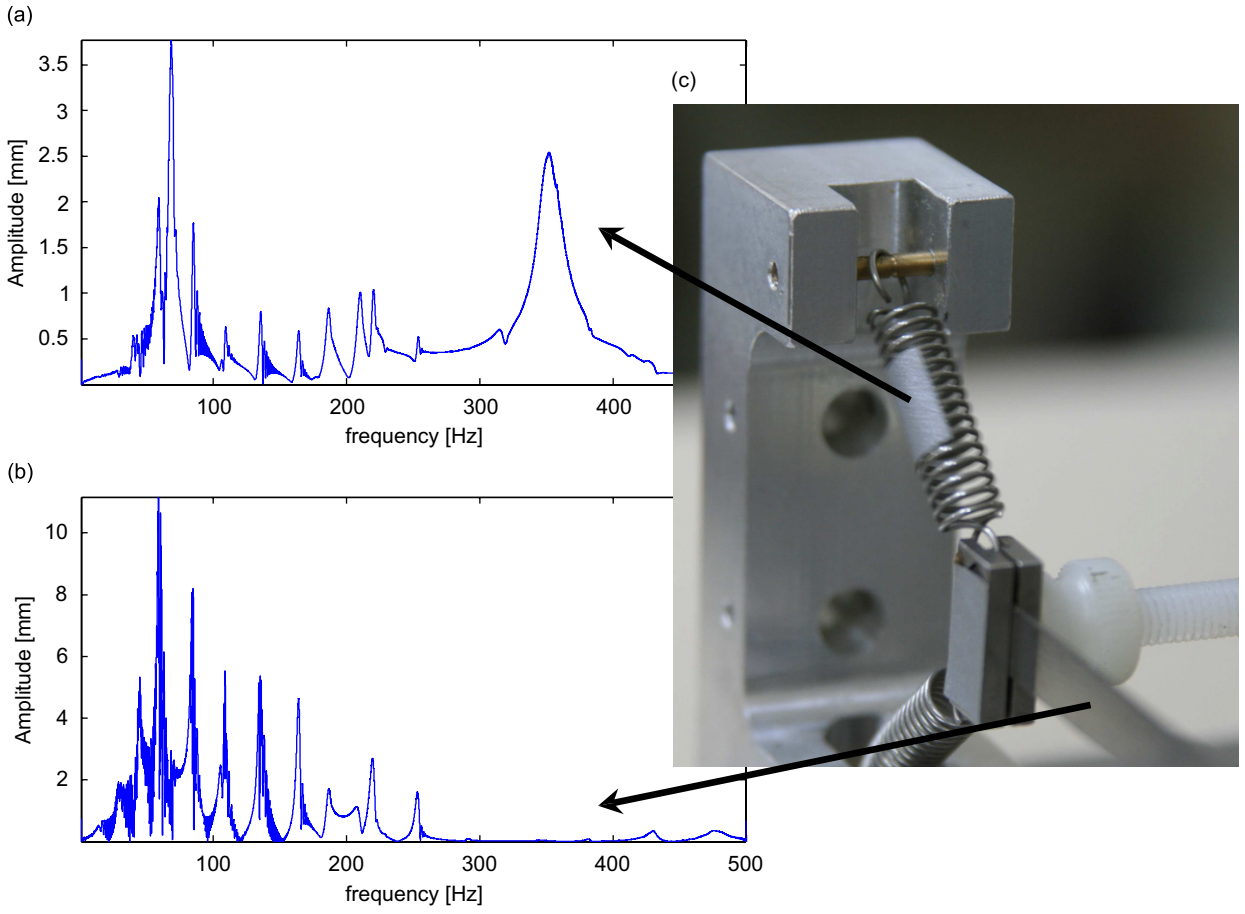

Fig. 8. The measured frequency response: (a) the response measured on the edge spring, (b) the response measured on a point on the string and (c) photograph of the measured locations.

presented on Fig. 4(a). It is seen that the theoretical and experimental maps are far from being identical. The minimum points that represent the optimal amplitude and phase for a traveling wave are located at different locations on the maps. This further supports the conclusion from the previous section, stating that it is not possible to rely on the theoretical model to determine the forces that generate pure traveling waves. Nevertheless, a simple tuning phase achieves this goal in most cases.

5.2. Boundary effects

Fig. 7(d) shows the map for frequency of 353 Hz. In this frequency, the system behavior is similar to the behavior presented by the theoretical map on Fig. 4(d). It can be seen that the map has no minimum point within the power limitations of the system. Thus, it is not possible to generate a pure traveling wave at this frequency. Measuring the frequency response of the system on several points along the string and on the boundaries can explain this behavior. In Fig. 8, the frequency response is shown for a point on the string and for a point on the edge spring. It is evident that while the string's response to 353 Hz is rather weak, the edge spring's response, at this frequency, is quite high. This may suggest that a local natural frequency of the boundary occurs at this frequency. This case was addressed earlier in Section 3, Eq. (48). Most of the energy

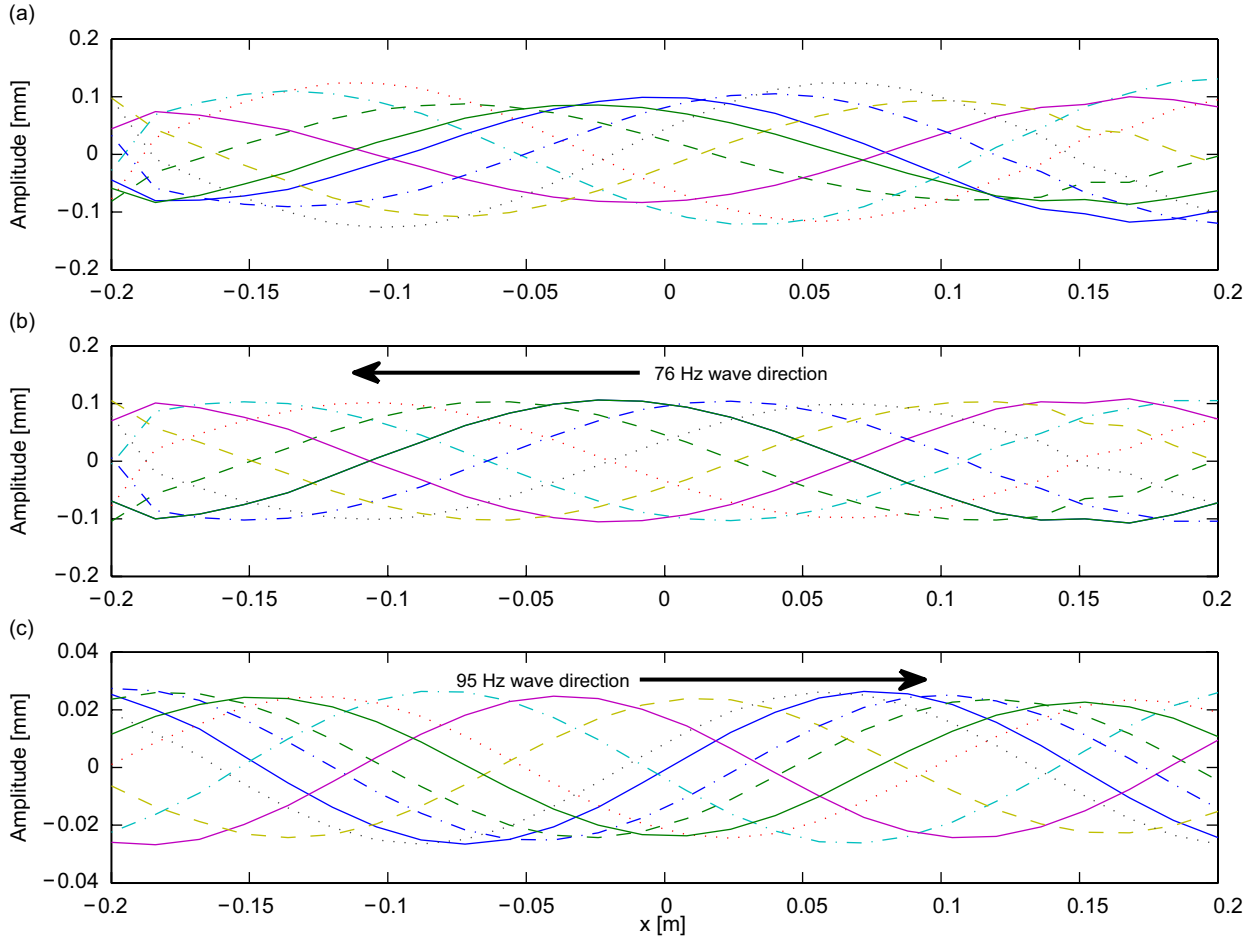

Fig. 9. The string response when tuned to have two traveling waves with different wavelengths having the frequencies—76 and 95 Hz. (a) The measured spatial response at growing successive time instances t_1-, t_2--, $t_3\ldots$, $t_4.-$. The decomposed string response from (a) the decomposition shows that there are two pure traveling waves oscillating at (b) 76 Hz wave and (c) 95 Hz wave.

which is injected at this frequency goes to the vibrations of the edge supports rather than to the string itself. The lack of sufficient power and the fear from causing permanent damage prevents us from achieving traveling waves.

5.3. Tuning multiple traveling waves using ESPRIT

Based on the maps for an excitation frequency of 76 and 96 Hz, it is possible to tune a traveling wave composed from a combination of the two frequencies, yielding a response containing two different wavelengths. The combined response is expected to contain two couples of wavenumbers, $(\pm\kappa_{76}, \pm\kappa_{95})$ where the sign indicates whether it progresses in the forward or backward direction. Once decomposed, each wavelength represents the response for a single excitation frequency (76 and 95 Hz, respectively). The cost function is evaluated as shown in Eq. (53) and optimized to obtain a pure traveling wave in each frequency. An initial guess for the different amplitude ratio and relative phase is formed based on the measured maps (see Fig. 7). Thus, only minor adjustments are expected by the optimization to overcome the non-linear effects between the two frequencies. In the presented experiment, the 76 Hz wave (normalized wavelength $\lambda_{76} = 0.45$) is traveling to the left $(-x)$ direction, and the 95 Hz wave (normalized wavelength of $\lambda_{95} = 0.38$) is traveling to the right $(+x)$ direction. A series of time instances of the measured spatial string response of the string (the response of the 0.4 m mid string section) for the two frequencies is shown in Fig. 9(a). An animation video of this response is provided in Electronic Annex 1. The composed response, which contains two uncoupled traveling waves, does not look like a traveling nor does it form a standing phenomenon. In Fig. 9(b) and (c), the response is decomposed into the two different waves with the ESPRIT based algorithm (an animation video is provided in Electronic Annex 2). It can be seen that each one of the separate waves is a pure traveling wave having a different wavelength, phase and amplitude.

6. Conclusions

In this paper, an active tuning approach to generate traveling waves in finite structures was investigated. Although in theory, it appears that a rather simple analytical expression for the external forces generates the desired traveling wave, in practice, it was shown here that the slightest inaccuracy in the mathematical model may render such an approach useless. It is therefore necessary to calibrate the external forces to fit the physical structure and to choose appropriate excitation frequencies. If not chosen wisely, the structure's dynamics can divert energy to localized regions for specific wavelengths, thus making the tuning progress unsuccessful. The tuning process presented in this paper is based on an on-line estimation of the waves from the measured structure response. In this work, the ESPRIT algorithm was used for the estimation task. The ESPRIT is a parametric algorithm with high resolution and with the ability to separate several waves from each other. This paves the way to handle structural responses that are composed from several traveling waves and tune each wave to travel independently. A series of experiments validating the results were carried out on a laboratory string-like structure.

Acknowledgments

This research was supported by The Israel Science Foundation (Grant no. 579/04).

The authors wish to thank Mr. Hadar Raz for his invaluable help in designing and building the experimental system.

Appendix A. Supplementary materials

Supplementary data associated with this article can be found in the online version at doi:10.1016/j.jsv.2008.06.013

References

[1] D.J. Mead, Wave propagation in continuous periodic structures: research contribution from Southampton, 1964–1995, *Journal of Sound and Vibration* 190 (1996) 495–524.

[2] M. Kuribayashi, S. Ueha, E. Mori, Excitation conditions of flexural traveling waves for a reversible ultrasonic linear motor, *Journal of the Acoustical Society of America* 77 (1985) 1431–1435.

[3] A. Minikes, I. Bucher, Non-contacting lateral transportation using gas squeeze film generated by flexural traveling waves—numerical analysis, *Journal of the Acoustical Society of America* 113 (2003) 2464–2473.

[4] L. Chen, Y. Wang, S. Ma, B. Li, Analysis of traveling wave locomotion of snake robot, *Proceedings of the 2003 IEEE, International Conference on Robotics, Intelligent Systems, and Signal Processing*, Changsha, China, October 2003.

[5] B.R. Mace, Wave reflection and transmission in beams, *Journal of Sound and Vibration* 97 (1984) 237–246.

[6] D.J. Pines, A.H. von Flotow, Active control of bending wave propagation at acoustic frequencies, *Journal of Sound and Vibrations* 142 (1990) 391–412.

[7] C. Mei, The analysis and control of longitudinal vibrations from wave viewpoint, *Journal of Vibration and Acoustics* 124 (2002) 645–649.

[8] P. Gardonio, S.J. Elliott, Active control of waves on a one-dimensional structure with a scattering termination, *Journal of Sound and Vibrations* 192 (1996) 701–730.

[9] S.J. Elliott, L. Billet, Adaptive control of flexural waves propagating in a beam, *Journal of Sound and Vibration* 163 (1993) 295–310.

[10] C.A. Tan, S. Ying, Dynamic analysis of the axially moving string based on wave propagation, *Journal of Applied Mechanics* 64 (1997) 394–400.

[11] C.H. Chung, C.A. Tan, Active control of the axially moving string by wave cancellation, *Journal of Vibration and Acoustics* 117 (1995) 49–55.

[12] A.J. Hull, A closed form solution of a longitudinal bar with a viscous boundary condition, *Journal of Sound and Vibration* 169 (1994) 19–28.

[13] B. Loh, P.I. Ro, An object transport system using flexural ultrasonic progressive waves generated by two-mode excitation, *IEEE Transaction on Ultrasonics, Ferroelectrics and Frequency Control* 47 (2000) 994–999.

[14] N. Tanaka, Y. Kikushima, Active wave control of a flexible beam (proposition of the active sink method), *JSME International Journal Series III* 34 (1991) 159–167.

[15] A. Minikes, R. Gabai, I. Bucher, M. Feldman, On the sensing and tuning of progressive structural vibration waves, *IEEE Transactions on Ultrasonics, Ferroelectrics and Frequency Control* 52 (2005) 1565–1576.

[16] R. Gabai, I. Bucher, On vibrating traveling waves actuation, sensing, and tuning, in finite structures. 2006 ASME International Mechanical Engineering Congress and Exposition, Chicago, Illinois, USA, November 5–10, 2006.

[17] I. Bucher, Estimating the ratio between traveling and standing vibration waves under non-stationary conditions, *Journal of Sound and Vibration* 270 (2004) 341–349.

[18] S.L. Marple, *Digital Spectral Analysis with Applications*, Prentice-Hall, 1987.

[19] R. Roy, T. Kailath, ESPRIT—estimation of signal parameters via rotational invariance techniques, *IEEE Transaction on Acoustics, Speech, and Signal Processing* 37 (1989) 984–994.

[20] P. Stoica, R. Moses, *Introduction to Spectral Analysis*, Prentice-Hall, 1997.

[21] I. Santamaria, C. Pantaleon, J. Ibanez, A comparative study of high-accuracy frequency estimation methods, *Mechanical Systems and Signal Processing* 14 (2000) 819–834.

[22] M.D. Zoltowski, M. Haardt, C.P. Mathews, Closed-form 2-D angle estimation with rectangular arrays in element space or beamspace unitary ESPRIT, *IEEE Transaction on Signal Processing* 44 (1996) 316–328.

[23] M.P. Norton, *Fundamentals of Noise and Vibration Analysis for Engineers*, Cambridge University Press, 1989.